Dalton Transactions

Accepted Manuscript

ROYAL SOCIETY OF CHEMISTRY

www.rsc.org/dalton

PAPER

Co_xC-encased carbon nanotube: an efficient oxygen reduction catalyst under both acidic and alkaline conditions

Received 00th January 20xx,
Accepted 00th January 20xx

DOI: 10.1039/x0xx00000x

www.rsc.org/

Lisong Chen[a], Xiangzhi Cui[a], Qingsong Wang[a], Xiaohua Zhang[a], Gang Wan[a], Fangming Cui[b], Chenyang Wei[a] , Jianlin Shi[a]*

The design of non-precious metal oxygen reduction reaction (ORR) catalyst of high activity and long durability in acidic electrolyte is of great importance for the development and commercialization of low-temperature fuel cells, which, however, remain a great challenge to date. Here, we demonstrate a facile, scalable protocol for the controlled synthesis of Co_xC-encapsulated carbon nanotubes as a novel kind of efficient electrochemical oxygen reduction reaction (ORR) catalyst. The synthesized Co_xC/carbon nanotube is featured with high BET surface area, large pore volume and high graphitic content, which greatly favors enhanced ORR properties. The resultant composite electro-catalyst shows high ORR activity which is comparable with that of 20wt% Pt/C in 0.1 M KOH electrolyte. More importantly, they also exhibit high ORR activity in 0.1 M $HClO_4$ with a near-complete 4e pathway. More attractively, compared to the most investigated Fe_xC, Co_xC as the proposed main catalytic active center shows much enhanced activity in acidic electrolyte, which will pave the way towards the rational design of advanced electro-catalyst for efficient ORR process especially in acidic conditions. Moverover, a fuel cell by using the synthesized Co_xC/carbon nanotube as cathode catalyst showed large open-circuit potential, high output power density and long durability, which make them a promising alternative for Pt/C as non-precious metal ORR catalyst in proton exchange membrane fuel cells.

1. Introduction

With the increasing demands for energy, limited earth storage of fossil fuels and the ever-severe environmental problem accompanying the fossil fuel consumption, it is extremely emergent to develop new kinds of sustainable energy supply. Proton exchange membrane fuel cells (PEMFCs) are one of the most promising clean energy sources with renewable hydrogen as fuel, especially for the booming automobile industry[1, 2]. However, the commercialization of PEMFCs was severely hampered by the high costs and scarcity of Pt based catalysts, especially for the oxygen reduction reactions (ORR) in the cathode in which 40wt% Pt/C was inevitably needed[1, 3, 4]. Accordingly, the development of cost-effective non-precious metal ORR catalysts with efficient activity becomes a foremost subject of the field.[5]

Various non-metal or non-precious metal catalysts have been reported, such as one or more kinds of non-metallic element (nitrogen[6-9], sulphur[10-12], boron[13, 14], phosphor[15] as well as fluorine[16]) doped carbon materials, C_3N_4 related materials[17, 18], M-N/C materials[19-21] (M = Fe, Co, Mn, N = non-metallic elements) or transition metal oxides, yet the results are far from satisfying because most of them only show moderate ORR activity and stability in alkaline solutions. Unfortunately, due to the much slower kinetics, a few types of materials showed limited ORR activity and in the meantime poor durability in acidic conditions. On the other hand, most reports of the non-precious metal ORR catalysts are limited to half-cell measurements, such as cyclic voltammetry (CV) and linear scanning voltammetry (LSV), the fuel cell performances of these catalysts under real working conditions are indeed rarely reported, which, however, are the much more important criterion for ORR catalysts.

Recently, confinement inside carbon nanotube is great effect on catalytic processes,[22-25] and carbon-coated iron carbide encased in carbon layers (Fe_xC/C) based electro-catalysts have been reported promising activity for oxygen reduction[26, 27], which is considered as a new type of catalytic sites for the electro-reduction of oxygen.[28] As far as we can find, there has been rare report to date about transition metal carbide encased in carbon layers composition based catalysts except for Fe_xC/C. Here, we report the synthesis of Co_xC encased in carbon nanotube by pyrolyzing a mixture of cobalt phthalocyanine coordinate and KIT-6 mesoporous silica with P123 surfactant inside the mesopore network. The synthesized

[a] State Key Lab of High Performance Ceramics and Superfine Microstructure, Shanghai Institute of Ceramics, Chinese Academy of Sciences, Shanghai, 200050, P. R. China. *corresponding author. E-mail: jlshi@mail.sic.ac.cn; Fax: + 86-21-52413122; Tel: + 86-21-52412712
[b] Qian Xuesen Laboratory of Space Technology, China Academy of Space Technology, Beijing, 100094, P. R. China.
† Footnotes relating to the title and/or authors should appear here.
Electronic Supplementary Information (ESI) available: [details of any supplementary information available should be included here]. See DOI: 10.1039/x0xx00000x

Co_xC/carbon nanotube shows excellent activities and high stabilities in both acidic and alkaline media. It should be noted that the synthesized Co_xC/carbon nanotube shows comparable ORR performance in alkaline solution to, and even higher activity than, Fe_xC/C in acidic electrolyte. Therefore, Co_xC as the active center should be more promising as an ORR catalytic active center than Fe_xC/C especially in acidic electrolyte. Moreover, the fuel cell assembled with the Co_xC/carbon nanotube as the cathode catalyst showed reasonably high output power density and long lifetime.

2. Experiment

2.1 Catalysts preparation

Mesoporous silica with cubic symmetry (Ia3d) was prepared following the procedure reported by Ryoo et al.[29]. Typically, 6 g of surfactant P123 and 6 g of n-butanol was dissolved in a solution of 217 g distilled water and 11.4 g HCl (37 wt.%). To this homogeneous solution, 12.9 g of tetraethylorthosilicate (TEOS) was added under stirring at 311 K and continuously stirred at 311 K for additional 24 h. The mixture was heated for 24 h at 373 K under static conditions for the hydrothermal treatment followed by filtration, washing, drying at 80 ^oC in air. The organic surface agent P123 was not removed and to be used as reactant during the synthesis of carbon nanotube.

To get Co_xC/C, 0.5 g CoPc was mechanically mixed with 0.5g KIT-6 with P123 inside the pores. And then, the mixture was put into tube furnace and pyrolysized under nitrogen flow at 800^oC for 10h. The resulted materials were treated by 2 M NaOH and 2 M HNO_3 both at 80^oC in turn to remove the silica and Co species. This purification product was collected by centrifugation and washed with distilled water and ethanol, and then dried at 80^oC in air. Fe_xC/C and Ni/C were also prepared for comparison by similar process while change CoPc to FePc or NiPc, respectively.

2.2 Physical characterization

The transition electron microscopy (TEM) images and energy-dispersive X-ray (EDX) spectra in this work were collected from a JEOL-2010F electron microscope operated at 200 kV. The powder X-ray diffraction (XRD) patterns of the as prepared samples were recorded on a Rigaku D/Max-2550 V X-ray diffractometer with a Cu Kαradiation target (40 KV, 40 mA), and the scanning rate was 4°per minute. X-ray photoelectron spectroscopy (XPS) signals were collected on a VG Micro MK II instrument using monochromatic Mg Ka X-rays at 1253.6 eV operated at 150 W. Raman spectra were recorded on a DXR Raman Microscope with a 532 nm excitation length, Thermal Scientific Co., USA. The nitrogen adsorption-desorption measurement was performed using Micromeritics Tristar 3000 at 77 K, and the specific surface area and pore size distribution were calculated using the Brunauer-Emmett-Teller (BET) and Barrett-Joyner-Halenda (BJH) methods, respectively.

2.3 Electrochemical characterization

All the electrochemical measurements were carried out on CHI 760E electrochemical workstation (CH Instrument, Inc.) with a standard three-electrode cell at room temperature. A platinum wire and Ag/AgCl (3 M KCl) were used as counter and reference electrodes, respectively. 0.1 M KOH or 0.1 M$HClO_4$ solution was used as electrolyte for electrochemical measurements. A Rotating ring-disk electrode (RRDE) with a Pt ring (4 mm inner-diameter and 6 mm outer diameter) and a glass carbon disk (6 mm diameter) served as the substrates for the working electrode for evaluating the ORR activity and selectivity of various catalysts. Prior to use, glassy carbon electrode was polished withalumina slurry (1.0 μm, 0.3 μm and 0.05 μm) in sequence, and ultrasonically cleaned thoroughly with pure water between each polishing step. Catalyst ink was prepared by blending catalyst power (10 mg) with 2 mL of mixed solution (ethanol: water = 1 : 1, volume scale) and 50μL Nafion solution (5%) in the ultrasonic bath.

a. CV test: 20 μL catalyst ink was transferred onto the glassy carbon substrate, yielding a catalyst loading level of 0.35 mg cm^{-2}. The catalysts were characterized by cyclic voltammetry (CV) test at room temperature. The CV curves were obtained by cycling scan after purging N_2 or O_2 for 15 min.

b. RDE test: Rotating disk electrode (RDE) measurement. Rotating disk electrode (RDE) measurements were performed with ALS-RRDE 3A Research Instruments. RDE measurements were carried out in the oxygen saturated 0.1M KOH or 0.1M $HClO_4$ at rotating rates varying from 400 rpm to 2025 rpm with the scan rate of 5mV s^{-1}. LSV on RDE was performed at the RDE of 3 mm in diameter.

c. RRDE test: Rotating ring-disk electrode (RRDE) measurement. Catalyst inks and electrodes were prepared by the same method above. The disk electrode was scanned at a rate of 5 mV s^{-1}. The electron transfer number n was calculated by the following equation (S1)

(S1) $$n=4\times\frac{I_d}{I_d+I_r/N}$$

The $\%HO_2^-$ was determined by the following equations (S2)

$$\%(HO_2^-)=200\times\frac{I_r/N}{I_d+I_r/N}$$

Where Id is disk current, Ir is ring current, and N is current collection efficiency of the Pt ring. N was determined to be 0.40 from the reduction of $K_3Fe(CN)_6$.

2.4 Membrane and electrode assembly (MEA) fabrication

Firstly, nafion 211 membrane (Dupont) was treated with 3 vol.% H_2O_2 and 0.5 M H_2SO_4 for 1 h, respectively, to remove impurities. The membrane was then washed several times with hot ultrapure water. Then, the catalyst ink was prepared by ultrasonically mixing the catalyst powder, 5 wt% Nafion solution (Dupon) and isopropanol for 30 min at 0^oC. The Nafion content in the dry catalyst layer was 33wt%. The catalyst ink was sprayed to carbon paper (Ballard GDS3260) with diffusion layer. The gas diffusion layer (GDL) consisted of teflonated carbon paper covered with a microporous layer made of carbon black and teflon. The loading of cathode with Co_xC/C was approximately 3.0mg/cm^2. The loading of anode with 20wt% Pt/C was 1.0mg/cm^2, which results in an absolute Pt loading 0.2mg/cm^2. The MEA was fabricated by hot-pressing the anode and cathode on each side of the pretreated Nafion 211 membrane (Dupon) at 135^o C and a pressure of 19MPa for 120 seconds.

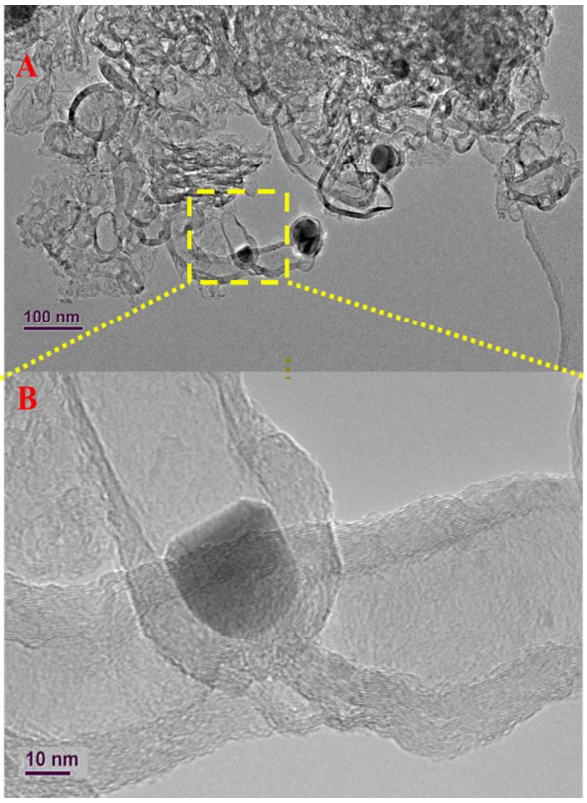

Fig. 1 TEM (A) and HRTEM (B) images of Co_xC/carbon nanotube

2.5 Single cell tests – activity and durability. The MEA with two silicon sheets was assembled into a single cell with graphite flow field plates and Au-coated steel end plates with heating rods. The single cell was installed on a Fuel Cell Testing Equipment (Scribner Corp. USA), which was equipped with mass flow-rate controllers and humidifiers for the reactant gases. The single cell was operated at 60 °C and the H_2/O_2 humidifier temperatures were 80 °C/80 °C. Pure H_2 and O_2 at a flow rate of 50 mL min^{-1} and 100 mL min^{-1} at 100% RH were fed into the anode and cathode, respectively. The pressure in the anode and cathode was 1.0 bar. Polarization curves were recorded by scanning the cell voltage from open circuit voltage down to 0.2 V at a scan rate of 0.5 mV s^{-1}. Then the fuel cell was hold at OCV again for 5 min. After that the current density was held at 70 mA cm^{-2} for duration and the cell potential was recorded.

3. Results and discussion

The synthesized samples were first observed using TEM. As can be seen in Fig. 1, carbon nanotubes are obtained by a facile copyrolysis process from a mixture of CoPc and P123-retained KIT-6 mesoporous silica inside the pores. Co-containing particles of about 10nm in diameter are encapsulated within carbon nanotubes, as can be found in the HRTEM image (Fig. 1B, Fig. S1 A~B), though several larger Co-

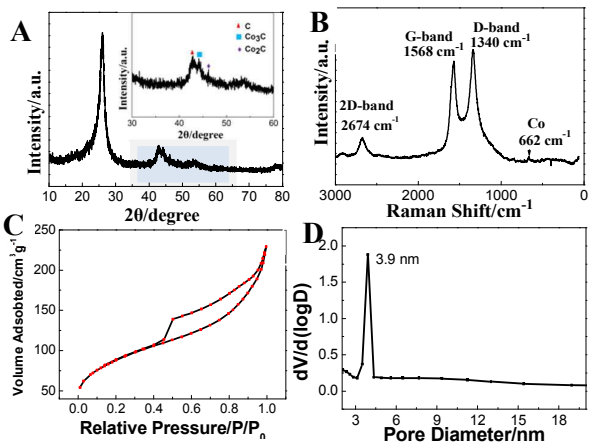

Fig. 2 (A) XRD pattern (the colored part from 30° to 60° is enlarged and inset into Fig. 2A), (B) Raman curve, (C) nitrogen adsorption-desorption isotherm and (D) the corresponding pore size distribution derived from the desorption branch

containing particles can be observed in Fig. 1A. According to the previous reports, Carbon layer in direct contact with CoxC in the present structure of CoxC nanoparticles-confined in CNTs will endow the catalyst with relatively lowered local work function and therefore higher activitycarbon layers[30]. Therefore, oxygen is likely to be adsorbed and reduced on these sites. On the other hand, the carbon layer encapsulation on CoxC nanoparticles can protect the transition metal nanoparticles from degradation in the harsh operation conditions of PEMFCs. Therefore, the structure with metal particles being encapsulated in carbon nanotubes of the synthesized Co_xC/carbon nanotube is desirable for the high activity and long life time of ORR catalysts. For comparison, the TEM images of Fe_xC/C and Ni/C are illustrated in Fig. S1. Fe_xC/C shows irregular morphology while Ni/C forms carbon nanotubes in a large scope. To know the element composition of the obtained samples, energy dispersive spectrum was recorded (Fig. S2). The signals of transition metal Co and Ni can be detected in Co_xC/C and Ni/C, respectively, while no significant iron element can be found in the sample of Fe_xC/C. This should be due to the fact that very low amount of Fe_xC encased in carbon layers in the prepared materials under these conditions. The Fe based compound is of high dissolubility, and the Fe element can be etched away in the acid washing process.

The XRD patterns of Co_xC/C in Fig. 2A indicate the presence of graphitized carbon, in which two weak peaks at about 26° and 43° can be found, corresponding to its (002) and (100) diffraction planes, respectively[7]. The peak at around 44.2° corresponds to Co_3C (JCPDS: 43-1144), and that at around 46.1° can be attributed to Co_2C (JCPDS: 50-1371), which can be seen more clearly in the enlarged XRD pattern inset into Fig. 2A. XRD patterns of the synthesized samples are compared in Fig. S3. All these three samples show typical graphite structure. Fe_xC/C shows a very weak XRD peak at

around 45° (JCPDS: 35-0772), while no clear peak belonging to nickel carbide can be found for Ni/C.

Fig. 2B shows the Raman spectrum of the Co_xC/C, with the three bands being at 1340, 1568, and 2674 cm^{-1}, corresponding to D band, G band and 2D band of graphite, respectively. The D and G bands are ascribed to the A_{1g} and E_{2g} modes of graphitic-like lattice vibrations[7, 31]. The I_D/I_G ratio, which is a commonly used figure of merit to gauge the

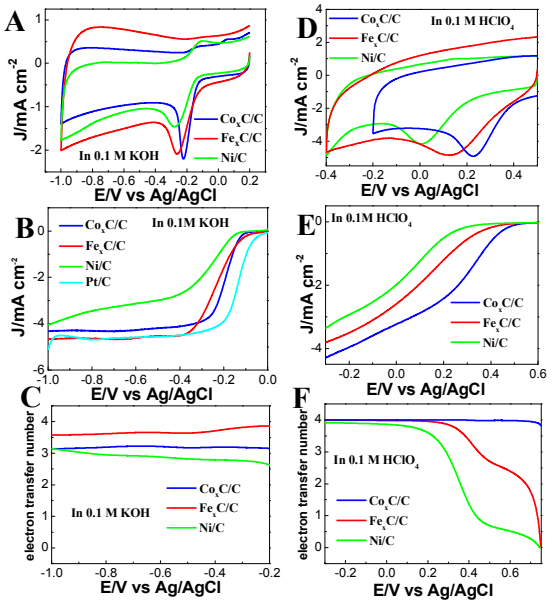

Fig. 3 CV curves of the synthesized samples in oxygen saturated 0.1 M KOH (A) or 0.1 M $HClO_4$ (D), LSV curves at the rotating speed of 1600 rpm of the synthesized samples in oxygen saturated 0.1 M KOH (B) or 0.1 M $HClO_4$ (E), electron transfer numbers of the synthesized samples during the oxygen reduction processes in oxygen saturated 0.1 M KOH (C) and 0.1 M $HCLO_4$ (F)

disordering degree of graphitic structure, is around 1.07 for the synthesized Co_xC/C. The disordered structure could result from the Co species loading and nitrogen doping in the synthesized samples, which are favorable for ORR. It should be pointed out that, the 2D band, corresponding to graphene layer, is rather sharp, indicating a few-layered graphene (<10 layers) present in the Co_xC/C. According to the previous report[30], the fewer the layer number is, the better ORR performance can be obtained. Similar Raman spectra of samples Fe_xC/C and Ni/C can also be found in Fig. S4. Notably, Co_xC/C shows the strongest 2D band intensity, suggesting the least carbon layer and possibly the highest electrochemical ORR activity.

The synthesized Co_xC/C manifests itself a porous structure as judged from the nitrogen adsorption-desorption isotherms (Fig. 2C) and the corresponding pore size distribution curves (Fig. 2D). Fig. 2C shows a typical type IV isotherm with a H3 hysteresis loop. Similar nitrogen sorption curves of Fe_xC/C and Ni/C can be seen in Fig. S5. The BET surface areas are 315, 906 and 376 $m^2\ g^{-1}$ for Co_xC/C, Fe_xC /C and Ni/C, respectively. The porous structure benefits oxygen transfer, and is thus favorable for ORR process. As can be seen in Fig. 2D and Fig. S5B, the synthesized samples all show uniform pore size distribution centered at 3.9 nm.

The ORR performance of the synthesized samples was initially investigated by cyclic voltammetry (CV) in 0.1 M KOH solution. As shown in Fig. S6, all three samples show quasi-rectangular voltammograms without redox peaks in nitrogen saturated electrolyte. While all samples display clear peaks corresponding to ORR in oxygen saturated 0.1 M KOH solutions (Fig.3A). Single oxygen reduction peak can be found at about -0.22V, -0.26V and -0.27V for Co_xC/C, Fe_xC/C and Ni/C, respectively. Similar trends can also be found in the LSV curves (Fig. 3B and Fig. S7). Although the onset potential of Fe_xC/C is a little positive than that of Co_xC/C, the half wave potential of Co_xC is obviously more positive. Electron transfer number is an important factor to evaluate ORR catalysts: a two electron pathway implies that H_2O_2 is the reaction product, meanwhile four electron pathway is featured with H_2O as reaction product. Since the membrane electrode assemblies are easy to be corroded by the resulted H_2O_2, leading to the decrease of life-time of fuel cells, therefore four electron transfer pathway is more favorable. It can be seen obviously from Fig. 3C, that both Fe_xC/C and Co_xC/C possess high electron transfer numbers (3.7~3.8e for Fe_xC/C and 3.2~3.3 for Co_xC/C) 0.1 M KOH solution.

Electrochemical performances in acidic solutions are much more attractive in practical applications. Attractively, all three samples demonstrate significant oxygen reduction peaks in their CV curves as can be seen in Fig. 3D and Fig. S8. Single oxygen reduction peaks occur at 0.22V, 0.13V and 0.01V for Co_xC/C, Fe_xC/C and Ni/C, respectively, and Co_xC/C shows the highest ORR potential, which is 90 mV and 210 mV higher than those of Fe_xC/C and Ni/C, respectively. RDE curves were also obtained in 0.1 M $HClO_4$ as shown in Fig. 3E and Fig. S9. RDE results tested in 0.1M $HClO_4$ solutions shows that, the Co_xC/C exhibits the most positive onset potential and the highest current density among these samples, indicating the highest ORR performance of Co_xC/C among the samples. Electron transfer number (Fig. 3F) was calculated from the RRDE result by equation S2. Sample Co_xC/C shows a nearly pure 4e reaction pathway in a large potential window from -0.1 V to 0.7 V, which is clearly higher than those of Fe_xC/C and Ni/C, especially at elevated potentials. As we have discussed above, although Fe_xC/C shows a comparable ORR activity with Co_xC/C especially in alkaline solution when compared with references[26, 27, 32], Co_xC/C is much more active than Fe_xC/C, namely, the former possesses more positive onset potential, much higher current density and a promising pure 4e reaction pathway.

As the catalytic activity of catalysts is closely related with their structures and chemical compositions, the synergistic cooperation between the compositions should be analyzed. According to the XPS analysis, all three samples show four kinds of element constituents, namely carbon, nitrogen, oxygen and transition metal (Table S1). As can be seen in Table

S1, similar content of N was doped into Fe_xC/C and Co_xC/C, and the N doped into carbon layers can decrease the local work function and increase the chemical reactivity of the carbon surface, therefore oxygen will be more easily adsorbed and reduced on the surface of carbon. However, the decrease of the local function and increase of chemical reactivity are still less effective to deconstruct the bond between oxygen atoms, especially in acidic environment. Therefore, what play the key role in the electrochemical ORR should be the carbide. The carbide encased in the carbon layers further activates the surrounding graphitic layers, making the carbon layers much active towards ORR, while the carbon layers can protect the carbide from acidic leaching and therefore keep the catalyst from losing its activity.[26] Moreover, Co_xC/C exhibits the highest ORR performance in acidic electrolyte among the synthesized samples, though it shows comparable ORR activity with Fe_xC/C in alkaline electrolyte. Co_xC, as the ORR main catalytic activity center, is here found to demonstrate much enhanced ORR activity as compared to Fe_xC, therefore will be more promising for future practical application.

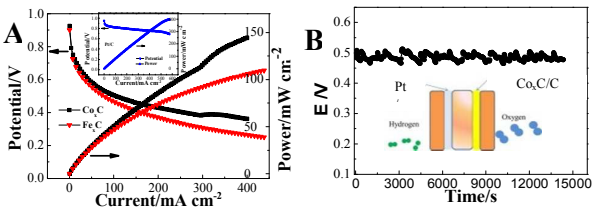

Fig. 4 (A) Polarization and power density plots for hydrogen-oxygen single fuel cell with Co_xC/C, Fe_xC/C, Pt/C (40wt%, JM) as cathode catalysts at 60°C; Nafion 211 membrane as electrolyte; cathode catalyst loading 3 mg cm^{-2}; Pt/C (20wt%, 3 mg cm^{-2} loading amount, JM) as an anode catalyst. No back pressure was applied. (B) Plot of Galvanostatic test at a fixed current density at 70 mA cm^{-2}

Importantly, a single PEM fuel cell by using synthesized Co_xC/C or Fe_xC/C (3 mg cm^{-2}) as cathode catalysts and commercial JM 20wt% Pt/C as anode catalyst (3 mg cm^{-2}, Pt loading 0.6 mg cm^{-2}) was assembled (named as Co_xC/C fuel cell and Fe_xC/C fuel cell, respectively) to test its single cell ORR performance and durability under real conditions. As illustrated in Fig. 4A, the Co_xC/C fuel cell shows a high open circuit voltage (0.93V) and high output power density (148 mW cm^{-2}) at 60°C under 100% RH hydrogen as anodic fuel and oxygen as cathodic oxidant, and no backpressure was applied. Single PEM fuel cell with commercial JM 40wt% Pt/C was also assembled (named as Pt/C fuel cell) for comparison under the same conditions, and the corresponding polarization and power density plot is inset into Fig. 4A. The output power density of Co_xC/C fuel cell, which has no precious metal on the cathode, accounts an almost 40% of that of all-Pt/C fuel cell. The Fe_xC/C fuel cell shows a similar open circuit voltage, but the output power density is obviously lower than that of Co_xC/C fuel cell. Then the Co_xC/C fuel cell was hold at the open circuit potential again for 5 min. After that the current density was held at 70 mA cm^{-2} for duration test and meanwhile the cell potential was recorded (Fig. 4B). In 15000 second, no voltage/power losses can be found, which is comparable or even better than literature reports[30, 32]. The LSV curves as well as the fuel cell performance indicate reasonably high activity and stability of CoxC/C towards ORR.

4. Conclusions

A Co_xC/carbon nanotube composite with Co_xC species being encapsulated in the carbon nanotubes has been synthesized by a facile co-pyrolysis method. Co_xC/C, as a new kind of ORR catalyst, shows high oxygen reduction performance in both acidic and alkaline solutions. Especially, Co_xC/C shows much higher/comparable ORR activities than/to Fe_xC/C in acidic and alkaline electrolytes, respectively. Single PEM fuel cell with Co_xC/C as cathodic catalyst shows a high open circuit potential, high output power density and long durability. The synthesized Co_xC/C can serve as a promising noble metal-free cathode ORR catalyst for PEM fuel cells.

Acknowledgements

The authors gratefully acknowledge the support of this research by National Key Basic Research Program of China (2013CB933200), National Natural Science Foundation of China (Grant No. 51202278, 51202288), Natural Science Foundation of Shanghai (12ZR1435200) and Key Laboratory of Functional Inorganic Material Chemistry (Heilongjiang University), Ministry of Education).

Notes and references

1. H. A. Gasteiger and N. M. Markovic, *Science*, 2009, **324**, 48-49.
2. M. K. Debe, *Nature*, 2012, **486**, 43-51.
3. Z. Chen, D. Higgins, A. Yu, L. Zhang and J. Zhang, *Energy & Environmental Science*, 2011, **4**, 3167-3192.
4. F. Jaouen, E. Proietti, M. Lefevre, R. Chenitz, J. P. Dodelet, G. Wu, H. T. Chung, C. M. Johnston and P. Zelenay, *Energy & Environmental Science*, 2011, **4**, 114-130.
5. Y. Nie, L. Li and Z. Wei, *Chemical Society Reviews*, 2015, **44**, 2168-2201.
6. K. Gong, F. Du, Z. Xia, M. Durstock and L. Dai, *Science*, 2009, **323**, 760-764.
7. L. Chen, X. Cui, L. Zhang, Y. Wang, M. Wang, F. Cui, C. Wei, J. Feng, T. Ge, W. Ren and J. Shi, *ChemSusChem*, 2015, **8**, 623-627.
8. H. W. Liang, X. Zhuang, S. Bruller, X. Feng and K. Mullen, *Nat Commun*, 2014, **5**, 4973.
9. G. Wu, N. H. Mack, W. Gao, S. G. Ma, R. Q. Zhong, J. T. Han, J. K. Baldwin and P. Zelenay, *Acs Nano*, 2012, **6**, 9764-9776.

10. Z. Ma, S. Dou, A. Shen, L. Tao, L. Dai and S. Wang, *Angewandte Chemie International Edition*, 2014, n/a-n/a.
11. Z. Yang, Z. Yao, G. Li, G. Fang, H. Nie, Z. Liu, X. Zhou, X. a. Chen and S. Huang, *Acs Nano*, 2012, **6**, 205-211.
12. L. Chen, X. Cui, Y. Wang, M. Wang, R. Qiu, Z. Shu, L. Zhang, Z. Hua, F. Cui, C. Wei and J. Shi, *Dalton Transactions*, 2014, **43**, 3420-3423.
13. S. Wang, E. Iyyamperumal, A. Roy, Y. Xue, D. Yu and L. Dai, *Angewandte Chemie-International Edition*, 2011, **50**, 11756-11760.
14. Y. Zheng, Y. Jiao, L. Ge, M. Jaroniec and S. Z. Qiao, *Angewandte Chemie-International Edition*, 2013, **52**, 3110-3116.
15. C. H. Choi, M. W. Chung, H. C. Kwon, S. H. Park and S. I. Woo, *Journal of Materials Chemistry A*, 2013, **1**, 3694-3699.
16. X. Sun, Y. Zhang, P. Song, J. Pan, L. Zhuang, W. Xu and W. Xing, *ACS Catalysis*, 2013, **3**, 1726-1729.
17. J. Liang, Y. Zheng, J. Chen, J. Liu, D. Hulicova-Jurcakova, M. Jaroniec and S. Z. Qiao, *Angewandte Chemie-International Edition*, 2012, **51**, 3892-3896.
18. Y. Zheng, Y. Jiao, J. Chen, J. Liu, J. Liang, A. Du, W. Zhang, Z. Zhu, S. C. Smith, M. Jaroniec, G. Q. Lu and S. Z. Qiao, *Journal of the American Chemical Society*, 2011, **133**, 20116-20119.
19. J. Du, F. Cheng, S. Wang, T. Zhang and J. Chen, *Scientific reports*, 2014, **4**.
20. Y. Wang, X. Cui, Y. Li, L. Chen, H. Chen, L. Zhang and J. Shi, *Carbon*, 2014, **68**, 232-239.
21. W. Xia, R. Zou, L. An, D. Xia and S. Guo, *Energy & Environmental Science*, 2015, **8**, 568-576.
22. X. Pan and X. Bao, *Accounts of Chemical Research*, 2011, **44**, 553-562.
23. A. Tavasoli, M. Trépanier, A. K. Dalai and N. Abatzoglou, *Journal of Chemical & Engineering Data*, 2010, **55**, 2757-2763.
24. D. Zhang, L. Zhang, L. Shi, C. Fang, H. Li, R. Gao, L. Huang and J. Zhang, *Nanoscale*, 2013, **5**, 1127-1136.
25. L. Zhang, D. Zhang, J. Zhang, S. Cai, C. Fang, L. Huang, H. Li, R. Gao and L. Shi, *Nanoscale*, 2013, **5**, 9821-9829.
26. Y. Hu, J. O. Jensen, W. Zhang, L. N. Cleemann, W. Xing, N. J. Bjerrum and Q. Li, *Angew Chem Int Ed Engl*, 2014, **53**, 3675-3679.
27. W. Yang, X. Liu, X. Yue, J. Jia and S. Guo, *Journal of the American Chemical Society*, 2015, **137**, 1436-1439.
28. J.-P. Dodelet, R. Chenitz, L. Yang and M. Lefevre, *ChemCatChem*, 2014, **6**, 1866-1867.
29. Y. Wang, X. Cui, Y. Li, L. Chen, Z. Shu, H. Chen and J. Shi, *Dalton Transactions*, 2013, **42**, 9448-9452.
30. D. Deng, L. Yu, X. Chen, G. Wang, L. Jin, X. Pan, J. Deng, G. Sun and X. Bao, *Angew Chem Int Ed Engl*, 2013, **52**, 371-375.
31. V. Di Noto, E. Negro, S. Polizzi, F. Agresti and G. A. Giffin, *Chemsuschem*, 2012, **5**, 2451-2459.
32. Y. Hu, J. O. Jensen, W. Zhang, S. Martin, R. Chenitz, C. Pan, W. Xing, N. J. Bjerrum and Q. Li, *Journal of Materials Chemistry A*, 2015.

Table of contents graphitic

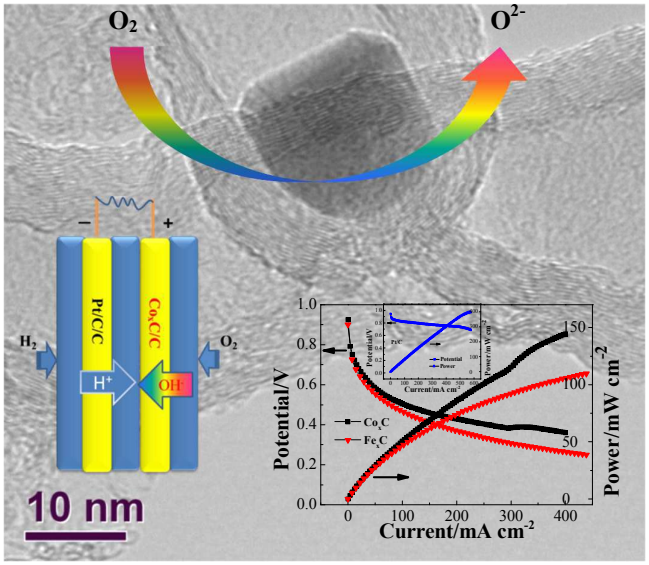

Co_xC encased in carbon nanotube were synthesized by a facile co-pyrolysis method and can be served as high efficient oxygen reduction catalysts under both acidic and alkaline conditions.